AIAA JOURNAL
Vol. 32, No. 3, March 1994

Quantitative Investigation of Compressible Mixing: Staged Transverse Injection into Mach 2 Flow

Steven D. Hollo,* James C. McDaniel,† and Roy J. Hartfield Jr.‡
University of Virginia, Charlottesville, Virginia 22903

Planar measurements of the injectant mole fraction distribution and the velocity field within a supersonic mixing flowfield have been made using laser-induced iodine fluorescence. The flowfield investigated in this work is staged transverse injection of air into a Mach 2 freestream. A complete three-dimensional survey of the injectant mole fraction distribution has been generated, and a single planar velocity measurement has been completed. The measurements reveal the dramatic effect of streamwise vortices on the mixing in the near field of the injectors, as well as the rapid mixing generated by staging two fuel injectors. Analysis of the downstream decay of the maximum injectant mole fraction in this and other supersonic mixing flowfields indicates that the relative rate of injectant mixing well downstream of the injectors is independent of injection geometry, freestream Mach number, and injectant molecular weight. Mixing within this region of the flowfield is dominated by small-scale turbulence within the injectant plume. The transition of the dominant mixing mechanism, from vortex-driven mixing in the near field to small-scale turbulent mixing in the far field, was found to occur in the region about 10 diameters downstream of the injectors.

Introduction

An understanding of the fundamental fluid mechanics of compressible mixing is vital to many current engineering applications, including gasdynamic lasers, aeroacoustics, and supersonic combustion. In a supersonic combustion ramjet (scramjet) engine, for instance, the extremely short residence time of the hydrogen fuel within the supersonic combustor makes rapid, controlled, and efficient fuel mixing critical to engine performance. Rapid mixing insures the shortest possible combustor length and maximizes the heat release from combustion, whereas a uniform distribution of fuel within the combustor optimizes combustion efficiency and minimizes the amount of air processed by the inlet that does not participate in combustion. Clearly, an understanding of the fundamental fluid mechanics of compressible mixing is essential to a successful supersonic combustor design.

The subject of this investigation is the experimental measurement of the injectant mole fraction distribution and the velocity field produced by staged transverse injection of air into a Mach 2 air flow. Figure 1 is a schematic of the flowfield produced by two circular injectors located along the centerline of the top wall of a Mach 2 constant area channel. The sonic injectors produce highly underexpanded jets that protrude into the freestream, giving rise to jet-induced bow shocks. The injectant mole fraction and velocity measurements made in this flowfield are used to investigate the fundamental mechanics of compressible mixing and the effect of staging two fuel injectors. An analysis of the downstream decay of the maximum injectant mole fraction is used to compare the relative mixing rates of different injection geometries and to determine the dominant mixing mechanism in different regions of the flowfield.

Presented as Paper 92-0093 at the AIAA 30th Aerospace Sciences Meeting, Reno, NV, Jan. 6–9, 1992; received March 28, 1992; revision received Aug. 12, 1993; accepted for publication Aug. 21, 1993.

*Research Scientist, Department of Mechanical and Aerospace Engineering. Member AIAA.

†Associate Professor, Department of Mechanical and Aerospace Engineering. Member AIAA.

‡Currently Assistant Professor, Department of Aerospace Engineering, Auburn University, Auburn, AL 36849. Member AIAA.

Measurement Techniques

Laser-induced iodine fluorescence (LIIF) is a nonintrusive and spatially resolved optical technique that has been used to make quantitative pointwise and planar measurements of pressure, temperature, density, and velocity in a variety of compressible flows.[1–4] Additionally, planar laser-induced iodine fluorescence (PLIIF) has been used to make measurements of the injectant mole fraction in supersonic mixing flowfields.[5–7] The technique described in Ref. 5 is used in this investigation to produce quantitative two-dimensional images of the injectant mole fraction distribution in the compressible mixing flowfield shown in Fig. 1. In compressible flows, the fluorescence signal resulting from laser excitation of iodine molecules seeded into the flowfield is strongly dependent on the thermodynamic state of the gas, the local laser power, and the local concentration of iodine molecules. The injectant mole fraction measurement technique eliminates the thermodynamic dependence of the fluorescence signal and the laser power variation within the planar laser sheet by taking the ratio of two fluorescence images: one collected with only the injectant seeded with iodine and a second with the entire flowfield seeded. The resulting ratioed image provides a quantitative measurement of the injectant mole fraction distribution in the plane probed by the laser sheet.[5]

The planar velocity measurement technique used in this investigation is based on measurements of the velocity-induced Doppler shift of the iodine absorption spectrum. Similar techniques have been used to make planar measurements in supersonic jets[1,2] and pointwise measurements in a compressible mixing flowfield.[4,8] In

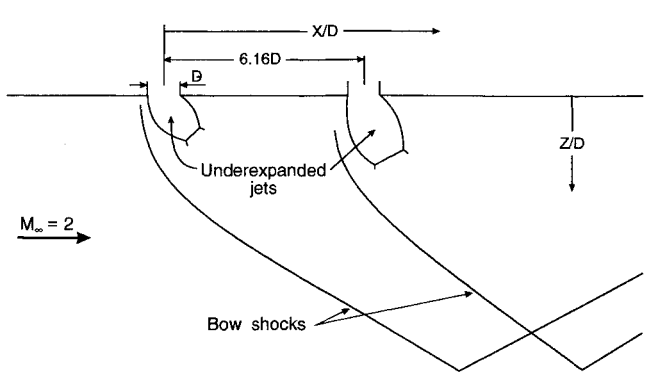

Fig. 1 Flowfield schematic.

Ref. 8, it was shown that an additional frequency shift in the iodine absorption spectrum caused by molecular collisions, the collisional impact shift, can be appreciable and must be accounted for in velocity measurements. The collisional shift can be eliminated by measuring the total frequency shift of the iodine spectrum using counterpropagating laser sheets[9] or by exploiting the symmetry of the flowfield to simulate counterpropagating laser sheets.[10,11] By exploiting flowfield symmetry, as done in the current investigation, the amount of spectral data that must be collected to measure the planar distribution of two velocity components is half that required by the counterpropagating laser sheets approach.

Experimental Setup and Procedure

The wind-tunnel facility used in this investigation was specifically designed for laser-induced iodine fluorescence measurements in compressible mixing flowfields. A two-dimensional Laval nozzle is used to develop continuous, shock-free, Mach 2 flow in a constant area rectangular test section, 1.81 cm in height and 2.92 cm in width. Two 2.06-mm circular injectors are located 12.7 mm apart along the centerline of the top wall of the test section. The bottom and side walls of the test section are made of fused silica to provide excellent optical access to the flowfield.

Iodine is seeded into the air supply in a large mixing vessel located upstream of the test section. The seeded air can be selectively routed either to the injectors only or to the injectors and the freestream simultaneously. Fluorescence of the iodine molecules is induced using a Spectra Physics Model 171 argon ion laser operated at 514.5 nm. The 514.5-nm line of the argon ion laser overlaps the strong P13, R15 absorption transitions of the (43–0) vibrational band of iodine. For the injectant mole fraction measurements, the laser is operated broadband at a nominal output power of 6 W. For the velocity measurements, the laser is operated with an air-spaced etalon inserted into the laser cavity to produce narrowband output. In both cases, the laser beam is converted into a 200-μm-thick sheet using a cylindrical and a spherical lens. The laser sheet is directed into the wind tunnel test section where it produces a thin plane of iodine fluorescence. The fluorescence is recorded using a Photometrics CH210 liquid-nitrogen-cooled CCD array camera (512 × 512 pixels with 14-bit resolution).

The planar velocity measurement consists of two linearly independent planar measurements of the total frequency shift of the iodine absorption spectrum. For each total frequency shift measurement, the single-mode output of the laser is tuned over a 5-GHz range by manually tilting the intracavity etalon. At each discrete laser frequency, a fluorescence image is recorded. The series of fluorescence images, properly normalized to account for the variation in laser power during the scan, is a record of the iodine absorption spectrum at each point in the flowfield. The total frequency shift of the absorption spectrum, relative to the unshifted spectrum measured in a static cell, is determined at each camera pixel by a computer program that employs a nonlinear curve-fitting routine to locate the transition line centers. Two planar total frequency shift measurements, conducted using orthogonal laser sheet directions, are sufficient to eliminate the collisional shift and to determine two linearly independent velocity components at every point in a flowfield symmetry plane.[10,11] Application of this technique is very time intensive; therefore, only a single planar velocity measurement was made in the course of this investigation. The technique is currently being automated to make complete surveys of complex three-dimensional velocity fields practical.

Results and Discussion

The injectant mole fraction and velocity measurements presented in this section utilize a cartesian coordinate system with the origin located at the center of the first injector. The x axis points downstream, the y axis points laterally across the test section, and the z axis is normal to the injector wall. Distances are normalized by the diameter of the injectors (2.06 mm). The wind-tunnel stagnation pressure and temperature for both the injectant mole fraction and velocity measurements were 262 kPa and 296 K, respectively. The injector stagnation pressure was 252 kPa. The measured mass flow rate and discharge coefficient of each injector were 1.75 g/s and 0.89, respectively. The tunnel mass flow rate was 0.18 kg/s. The boundary-layer thickness at the entrance to the test section is approximately 1.8 mm.[12] Complete measurements of the test section inlet and injector exit velocity profiles are presented in Ref. 13.

Injectant Mole Fraction Measurements

Figure 2 shows the injectant mole fraction distribution measured in the centerline penetration plane ($Y/D = 0$). The freestream flow is from left to right, and injection is from the top. The straight lines show the location of the top and bottom walls of the test section. The two underexpanded jet cores are clearly visible as regions of 100% injectant, whereas the edge of the injectant plume is delineated by the 2% contour line. The remaining contour lines clearly show the extent of injectant mixing as the plume is swept downstream. The second injector jet core penetrates further into the flow because it is shielded from the freestream momentum by the upstream jet. Another interesting feature of the penetration image is the small region of injectant upstream of the first injector. This suggests the existence of a small recirculation region within the boundary layer in front of the first jet.

Figure 3 shows the injectant mole fraction distribution in the spreading plane half a jet diameter from the injector wall ($Z/D = 0.5$). (The planar velocity measurement presented in the next section was also conducted in this plane.) The width of the contour plot is approximately 33% of the full width of the test section. This represents an area 1.0 cm wide centered on the test section's centerline. As expected, the circular injectors produce blunt, underexpanded jet cores that generate large disturbances in the flow. This leads to significant lateral spreading of the injectant near the wall. Significant mixing of the injectant occurs just downstream of the first injector. The shape of the 40 and 50% injectant contours is a result of the streamwise vortices generated as the freestream is forced around the jet core and up into the plume. (This effect is best visualized in the crossflow injectant mole fraction images and the planar velocity measurement presented later.) The majority of the injectant from the downstream injector penetrates further from the wall before significant mixing with the freestream begins.

Figure 4 contains contour plots of the crossflow injectant mole fraction distributions measured at eight locations within the test section. (A total of 24 crossflow images were generated in this injector geometry.) The contour plots show an area 2.16 cm wide by 1.15 cm high. This represents 45% of the total cross sectional area of the duct. The contour levels range from 100% to 10% injectant

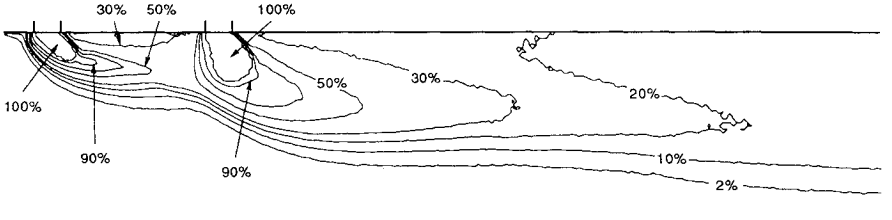

Fig. 2 Injectant mole fraction distribution in the centerline penetration plane ($Y/D = 0$).

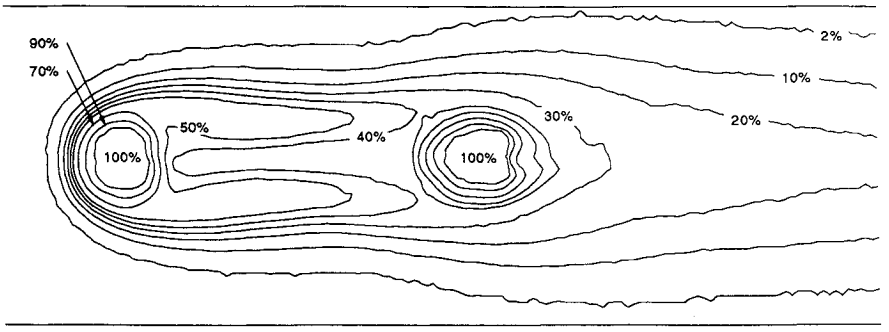

Fig. 3 Injectant mole fraction distribution in the spreading plane half a diameter from the injector wall ($Z/D = 0.5$).

in increments of 10%. The 2% injectant contour is also included to outline the edge of the plume.

The first crossflow plane shown in Fig. 4 is located at the center of the first injector, $X/D = 0$. This measurement plane shows the cross section of the underexpanded jet core and the steep gradient in the injectant concentration between the edge of the jet core and the freestream. The second crossflow plane, located two jet diameters downstream of the first injector centerline, begins to show the influence of the streamwise vortices generated as the freestream is forced around the underexpanded jet core. The vortices drive freestream air inward between the top wall and the injectant plume and then down into the injectant plume. Evidence of this effect is seen in the U-shaped contours near the wall, the pinched shape of the 2% contour between the boundary layer and the plume, and the characteristic kidney shape of the injectant plume. In the plane four diameters downstream of the first injector, $X/D = 4$, the action of the vortices has split the plume into two regions of high injectant concentration by driving freestream air down into the center of the plume. The fourth crossflow plane, $X/D = 6$, intersects the second injector jet core. The increased penetration of the second jet core is immediately obvious. The remaining four crossflow planes show the development of the plume downstream of the second injector to the end of the test section. The effect of the streamwise vortices downstream of the second injector is similar to but less dramatic than that seen downstream of the first injector. Evidence of the effect of the streamwise vortices is seen in the kidney-shaped 30% contour in the measurement plane at $X/D = 14$. The last crossflow plane in the sequence, $X/D = 30$, shows a large well-mixed, circular plume that has lost most of its upstream vortical history. Mixing in this downstream region of the plume is apparently dominated by small-scale turbulence instead of the coherent vortical structures that dominate mixing in the near field of the injectors. This observation is substantiated by the mixing rate data in the next section.

Mixing Rates

The crossflow injectant mole fraction images contain a wealth of information; however, it is often desirable to represent the data in a simpler form to facilitate comparisons of different injector geometries. One important parameter that can be investigated in this way is the mixing rate. A measure of the mixing rate that has been used in previous investigations is the downstream decay of the maximum injectant mass fraction.[14] For the experiments presented here, where the injectant and the freestream gases are identical, the injectant mole fraction and the injectant mass fraction are equivalent. Therefore, the decay of the maximum injectant mole fraction is used in this work as an indication of the injectant mixing rate. In the figures presented later, the maximum injectant mole fraction χ_{max} in each crossflow plane is plotted vs the nondimensional location of the measurement plane downstream of the injector.

Figure 5 shows the decay of the maximum injectant mole fraction downstream of the staged injectors. For comparison, the decay of χ_{max} downstream of a single circular injector, operated at the same total pressure as the staged injectors, is shown.[11] In this figure, the data points are connected by line segments to illustrate trends; data points within the jet cores are omitted. A significant difference in the initial rate of injectant mixing downstream of the single and staged injectors is evident. In the single injector geometry, the decay of the maximum injectant concentration is initially slow. In the staged geometry, however, both the first and second injectors produce rapid initial mixing of the injectant. This difference indicates that the presence of the second jet effects the rate of injectant mixing downstream of the first injector. If, due to the supersonic nature of the flowfield, for example, there were no upstream influence of the second jet in the staged geometry, then the initial mixing downstream of the first injector should match that of the single injector. This is clearly not the case; therefore, a strong subsonic flow interaction between the staged jets must be responsible for the increased mixing downstream of the first injector. The rapid mixing downstream of the second injector is due to the interaction between the jets, as well as the strong vortices generated by the larger underexpanded jet core of the second injector. The advantage of staging the injectors is evident: compared with the single injector, the staged injectors mix twice as much injectant to a lower maximum concentration within the length of the test section.

The decay of the maximum injectant concentration can also be presented on a log-log plot to give a useful indication of the rate of injectant mixing well downstream of the injectors. Previously, it has been found that, far downstream of the injectors, the data generally falls along a straight line in such a plot; therefore, the decay of the maximum injectant concentration far downstream of the injector can be written as

$$\chi_{max} \propto \left(\frac{X}{D}\right)^{-n} \tag{1}$$

where $-n$ is the slope of the line fitted to the far-field mixing data.[14] Taking the logarithmic differential of Eq. (1) gives

$$\frac{d\chi_{max}}{\chi_{max}} = -n\frac{d(X/D)}{(X/D)} \tag{2}$$

The value of n can be used to compare the relative far-field mixing rates of different injector configurations. A higher value of n indicates a faster relative rate of far-field injectant mixing. The regime in which this relationship applies has not been well defined since very little data in the near field of the injectors have been previously reported due to the inability of intrusive probes to make accurate measurements in this region.

Figure 6 shows the decay of the maximum injectant mole fraction for four injection geometries on a log-log plot. These four geometries—single injector, staged injectors at Mach 2, staged injectors at Mach 3, and staged injectors behind a rearward-facing step at Mach 2—were investigated using the same experimental setup and procedure described earlier.[7,11,13] The tunnel and injector stagnation conditions for all of the Mach 2 cases are the same as those reported earlier. The Mach 3 measurements were made using a different nozzle/test section with tunnel and injector stagnation pressures of 1.1 MPa and 241 kPa, respectively. For the staged injector geometries, the data are plotted vs the distance downstream of the second injector.

Several conclusions about relative mixing rates can be drawn from the data presented in Fig. 6. As discussed earlier, staging two fuel injectors increases the near-field rate of injectant mixing due to the interaction between the two jets. A comparison of the staged injector geometry at Mach 2 and 3 reveals that increasing the freestream Mach number decreases the overall rate of injectant mixing. The higher freestream velocity at Mach 3 increases the length over which the vortex mixing of the plume takes place. The staged injectors behind a rearward-facing step at Mach 2 produce the highest initial rate of injectant mixing. The partial shielding of the injectors by the step leads to greater jet penetration, which produces stronger streamwise vortices and faster mixing. The most striking feature in Fig. 6, however, is the nearly identical slope of each of the data sets well downstream of the injector. This indicates that the relative rate of injectant mixing in the far field is similar for all four flowfield configurations. The values of n, determined by power-law curve fits of the decay of χ_{max} in the far field, are given in Table 1 for all four flowfield configurations. The curve fits are shown in Fig. 6 (the length of the lines show the range of data over which the curve fits were calculated). The curve fits of the data downstream of the staged injectors at Mach 2 and the staged injectors behind a step are quite good. The curve fits to the data downstream of the single injector at Mach 2 and the staged injectors at Mach 3 are less conclusive due to the limited number of data points in the far-field region of these flowfields. In all four cases, however, the data suggest a transition to a dominant mixing mechanism that is insensitive to the injection geometry and the freestream Mach number.

As shown in Fig. 6, the decay of χ_{max} is a sensitive indicator of the dominant mixing mechanism. In the injector near field, the vortices shed by the jet core drive freestream air into the plume. This is responsible for the rapid initial drop in χ_{max} downstream of the injectors as seen in Fig. 5. As seen in Fig. 6, mixing in this region of the flowfield is strongly affected by injector geometry and freestream Mach number. As the plume grows, however, the strength of the vortices decreases. As a result, the impact of vortex mixing on the decay of the maximum injectant concentration diminishes. Well downstream of the injectors, the weak remnants of the vortices have very little effect on the rate of injectant mixing in the center of the plume. Here, the rate of decay of χ_{max} is governed by the rate of small-scale turbulent mixing within the plume and is insensitive to injection geometry and freestream Mach number.

The data presented in Fig. 6 suggest that the transition of the dominant mixing mechanism, from large-scale vortex-driven mixing in the near field to small-scale turbulent mixing in the far field, occurs in the region approximately 10 jet diameters downstream of

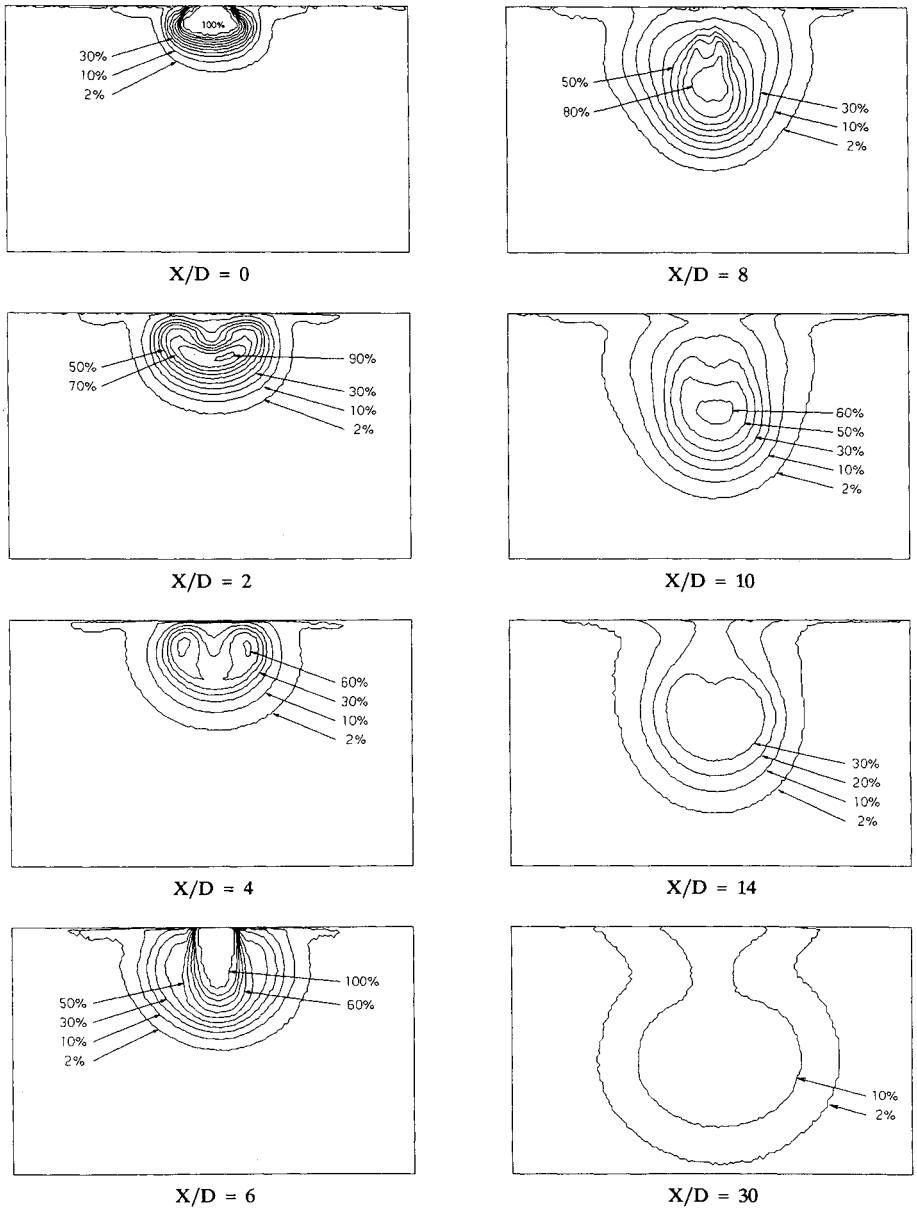

Fig. 4 Crossflow injectant mole fraction distributions.

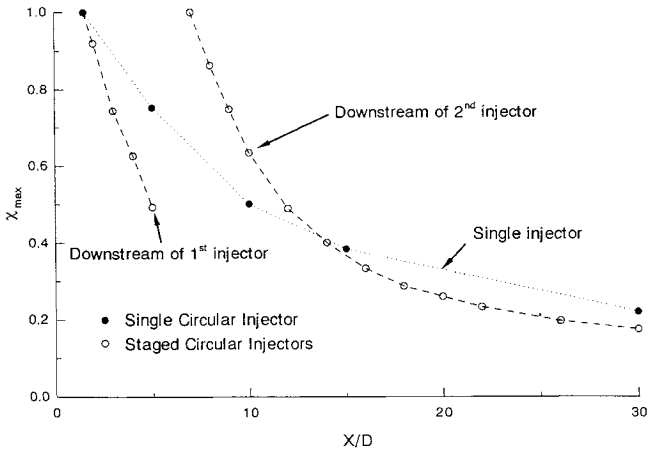

Fig. 5 Downstream decay of the maximum injectant mole fraction.

Table 1 Comparison of the relative far-field mixing rate for several different injection configurations.

Configuration	M_∞	Injectant	Slope, n
Single injector	2.0	Air	0.74
Staged injectors	2.0	Air	0.75
Staged injectors	2.9	Air	0.75
Staged injectors behind step	2.0	Air	0.69
Single injector[15]	4.0	H_2	0.8

the injectors for the Mach 2 freestream. The one data set at Mach 3 suggests that the transition region moves downstream with increasing freestream velocity. In the figure, the power-law curves show the region in which the relative decay of χ_{max} is insensitive to the configuration of the combustor. Upstream of this region, the mixing rate is very sensitive to combustor geometry. The approximate location of the transition between these two regions is suggested by the first data point included in the power-law curve fit for each data set. (The curve fits, shown in Fig. 6, were performed using a commercially available software package. The number of data points used for each fit was chosen, based on a degree-of-freedom adjusted r^2, to give the best fitting power-law curve for each data set. In all four cases, adding the next upstream data point to the curve-fit calculation seriously degrades the goodness-of-fit. The furthest upstream data point included in each curve fit, therefore, gives a reasonable indication of where the transition of the dominant mixing mechanism occurs.) Based on the data presented in Fig. 6, it is reasonable to conclude that the dominance of vortex-driven mixing is limited to the region 10 diameters downstream of the injector for the Mach 2 freestream. Downstream of this region, small-scale turbulent mixing governs the rate of injectant mixing within the plume.

The results presented in this section are similar to data generated during previous investigations of transverse injection into a supersonic freestream. Most notable are the investigations by Rogers[15,16] of hydrogen injection from single and multiple side-by-side circular injectors. Although the flowfield conditions were significantly different ($M_\infty = 4$, H_2 injectant), the data exhibit similar trends to those discussed earlier. In the far field (four points at $X/D \geq 30$), the decay of the maximum injectant concentration falls along a straight line on a log-log plot. In the near field (i.e., one data point at $X/D = 7$), however, the data consistently fall below this line. This is consistent with the conclusion that the transition from the near field to the far field occurs in the region around 10 diameters downstream of the injector for these types of low-enthalpy supersonic mixing flowfields. For the single hydrogen injector investigated by Rogers, a value of $n = 0.8$ was reported for the data in the far field. The similarity of this data with that presented in this paper suggests that the relative rate of injectant mixing in the far field is insensitive to both the freestream Mach number and the injectant molecular weight. In addition, the relative thickness of the boundary layer may have little effect on far-field mixing. In the investigation by Rogers, the boundary-layer thickness was 2.7 times the diameter of the injector. In this investigation, however, the boundary layer thickness is smaller than the diameter of the injectors ($\delta \approx 0.9D$).

Velocity Measurements

A single planar velocity measurement was conducted in the Mach 2 staged injector flowfield. The measurement was performed in the spreading plane with the laser sheet half an injector diameter ($Z/D = 0.5$) from the injector wall. This is the same plane in which the spreading injectant mole fraction image, presented in Fig. 3, was generated. The high degree of symmetry of the flowfield in this plane, a prerequisite of the velocity measurement technique, is apparent in the injectant mole fraction image. The location of the measurement plane near the wall was chosen to visualize the interaction of the main flow with the underexpanded jet cores produced by the injectors.

From the data contained in the fluorescence images it is possible to calculate the velocity components at approximately 80,000 points in the measurement plane. This amount of data is virtually impossible to present in a clear and useful vector plot. For this reason, it is necessary to present the velocity data at reduced resolution within multiple areas of interest in the flowfield. In this paper, three areas of interest are presented: two high-resolution closeups showing the velocity field in the regions around each injector and a low-resolution view of the entire velocity field overlaid with the injectant mole fraction measurement presented in Fig. 3.

Figure 7 is a vector plot of the velocity field in the vicinity of the first injector. The semicircle shows the size and location of the injector. The left edge of the plot shows the undisturbed flow upstream of the injectors. The core of the underexpanded jet produced by the circular injector is visualized by the radial expansion of the velocity vectors away from the center of the injector. In this plot, the approximate location of the barrel shock associated with the edge of the underexpanded jet core is visible along the injector centerline as the sudden decrease in the length of the velocity vectors. On the upstream side of the jet core, the barrel shock is in about the same location as the edge of the injector. On the downwind side of the jet core, the barrel shock is farther downstream than the edge of the injector. The expansion of the jet core is greater in the downstream direction due to the lower pressure on the downwind side of the jet. Within the jet core, the flow velocity is predominantly normal to the flow. In the center of the jet, the measured velocity is essentially zero, as expected. This illustrates the ability of the velocity measurement technique to accurately measure small velocity components. The location of the bow shock is implied by the small vectors just upstream of the jet core. However, it is clear from the slight deflection of the velocity vectors further upstream that the influence of the jet is not confined to

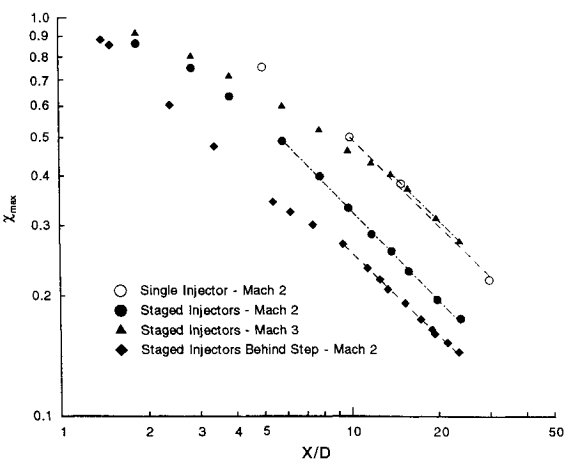

Fig. 6 Comparison of the downstream decay of the maximum injectant mole fraction for four different injection configurations. The dashed lines show power-law curve fits to the far-field data.

the region behind the bow shock. This can be attributed to the interaction of the bow shock with the boundary layer and to the presence of a small recirculation zone in front of the injector. A small recirculation bubble in front of the first jet core creates a weak separation shock upstream of the injector. This accounts for the deflection of the velocity vectors well upstream of the jet core. Evidence of a small recirculation region in front of the first circular injector was also seen in the penetration injectant mole fraction image. Downstream of the injector, the measured velocity is quite high everywhere except in the region immediately behind the jet core. In this region, the velocity is predominantly normal to the measurement plane.

Figure 8 is a vector plot of the measured velocity vectors in the near field of the second circular injector. The velocity field upstream of the jet core shows the effect of the expansion around the upstream jet. One of the most interesting aspects of the velocity field in this region is the low speeds measured directly in front of the jet core. In a large region just upstream of the second jet, the measured two-dimensional velocity is less than 300 m/s. This corresponds to a speed lower than Mach 1 (approximately 315 m/s with $T_0 \approx 296$ K). In addition, there is no evidence of the presence of a bow shock in the region directly in front of the jet core. This indicates that the flow in this region may be subsonic (recall that the vertical velocity component is not measured). The presence of a large subsonic region upstream of the jet core would certainly affect the rate of injectant mixing in the region between the injectors as discussed in the preceding section.

The interaction of the freestream with the underexpanded jet cores is graphically illustrated in the figures. In front of each jet, the freestream reaches what is best described as a pseudostagnation point, since the magnitude of the velocity component normal to the measurement plane is unknown. (Computational fluid dynamics calculations of a similar flowfield indicate that the speeds in these regions of the flow are indeed quite small.[17]) The deflection of the main flow around the jet cores is apparent. Directly in front of the first injector jet core, the freestream turns and slows rapidly. This gives an indication of the location of the first bow shock. Upstream of the second injector, however, the measured velocity is quite low and there is no evidence of a bow shock directly in front of the second jet core. On the downstream side of the underexpanded jet cores, the measured velocity is quite high. Downstream of the second injector the highest measured speed (two dimensional) is almost 600 m/s. These high speeds are produced as the flow expands into the regions behind the underexpanded jet cores. As discussed in the preceding section, this generates the streamwise vortices that dominate the near-field mixing of the injectant. As the flow spills around the jet core, freestream air is driven between the wall and the injectant plume. As this flow nears the centerline, it is forced away from the wall and into the center of the injectant plume. This results in rapid mixing of the injectant and the freestream as shown in the crossflow injectant mole fraction images.

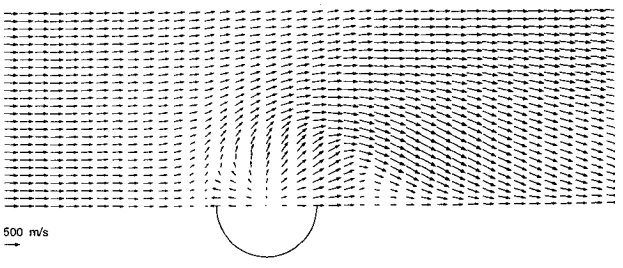

Fig. 7 Closeup of the velocity field near the first injector (Z/D = 0.5).

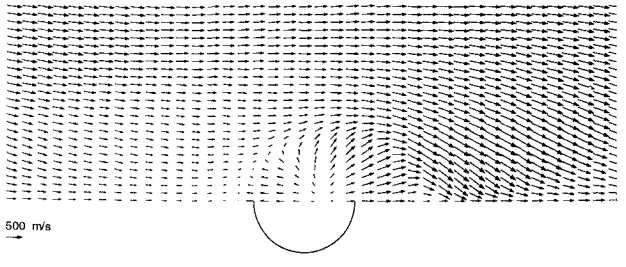

Fig. 8 Closeup of the velocity field near the second injector (Z/D = 0.5).

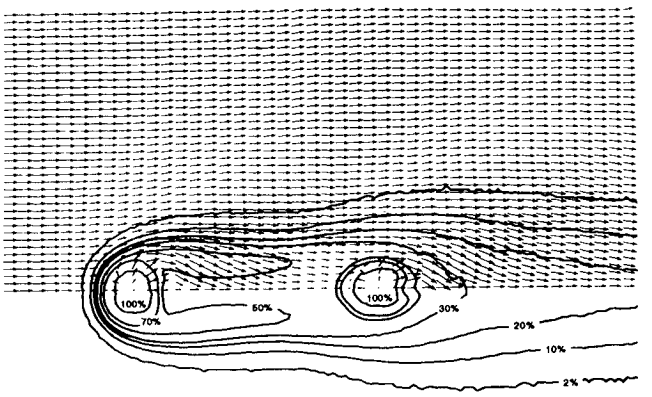

Fig. 9 Injectant mole fraction and velocity field composite (Z/D = 0.5).

Figure 9 is a composite of the velocity field and the injectant mole fraction distribution measured in the staged injector geometry. This plot shows how the velocity field affects the distribution of the injectant and the shape of the plume. The blunt shape of the first circular injector produces significant lateral spreading of the injectant. Downstream of both injectors, it is clear how the velocity field drives fluid with relatively low injectant concentrations inward and then up into the center of the plume. This effect is responsible for the horseshoe shape of the 50% contour line downstream of the first injector. In general, the injectant mole fraction contours that define the plume shape are tangent to the velocity field. For example, the expansion of the flow into the region behind the second jet core causes a corresponding contraction of the injectant plume.

The first column of velocity vectors in Fig. 9 corresponds to the location of the nozzle exit. Here the velocity distribution is relatively uniform and the flow is parallel to the test section centerline. The measured average streamwise velocity is approximately 478 m/s (U/U_∞ = 0. 930). This is lower than the Mach 2 freestream velocity of 515 m/s since the measurement plane (Z/D = 0.50) was located within the boundary layer. Previous laser Doppler anemometry (LDA) measurements of the velocity profile at the nozzle exit showed that the turbulent boundary layer is approximately 1.8 mm thick ($\delta/D \approx 0.9$) at the entrance to the test section and that the measured streamwise velocity at Z/D = 0.5 was 484 m/s (U/U_∞ = 0. 933).[12] (The normalized velocity component U/U_∞ eliminates the effect of the slightly different stagnation temperature of each experiment and is, therefore, more appropriate for direct comparison.) The extremely good agreement of the LDA and PLIIF velocity measurements is an indication of the accuracy of the PLIIF velocity measurement technique. The uncertainty in the velocity measurements is primarily dependent on the width of the iodine absorption line and was calculated to be less than ±10 m/s.

Summary and Conclusions

Extensive measurements of the injectant mole fraction distribution and the velocity field produced by staged transverse injection of air into a Mach 2 flow have been completed. This data set was used to analyze the fundamental mechanics of compressible mixing. An analysis of the downstream decay of the maximum injectant mole fraction was used to compare the relative mixing rates

of different injection configurations and to determine the dominant mixing mechanism in different regions of the flowfield.

The crossflow injectant mole fraction measurements vividly illustrate the effect of streamwise vortices on injectant mixing in the region just downstream of the injectors. The vortices are generated as freestream air spills around the underexpanded jet cores produced by the injectors. The vortices promote rapid mixing of the injectant by driving freestream air into the center of the plume.

The downstream decay of the maximum injectant mole fraction was used as an indication of the rate of injectant mixing. Comparisons of the data presented in this paper with previously published data reveal that staged injectors produce a significantly higher initial rate of injectant mixing than a single injector due to the strong subsonic interaction between the two jet cores. Shielding the injectors behind a rearward-facing step produces a further increase in the initial rate of injectant mixing. The higher freestream velocity at increased freestream Mach numbers, however, was shown to significantly reduce the initial rate of mixing. An analysis of the decay of the maximum injectant mole fraction revealed that the relative rate of injectant mixing in the far field of the injectors is similar for all of the injection geometries discussed in this paper. This indicates that the rate of small-scale turbulent mixing, the dominant mixing mechanism in the far field, is insensitive to the injection geometry, the freestream Mach number, and the injectant molecular weight. The analysis also suggests that, for transverse injection into low-Mach-number, low-enthalpy supersonic flows, the transition of the dominant mixing mechanism, from vortex-driven mixing in the near field to small-scale turbulent mixing in the far field, occurs in the region around 10 diameters downstream of the injectors.

The planar velocity measurement suggests the existence of a large subsonic region just upstream of the second injector. Such an interaction between the injectors would account for the dramatically increased mixing rate produced by the staged injectors compared with a single injector. The planar velocity measurement also illustrates how the streamwise vortices are formed and how the shape of the injectant plume is dictated by the velocity field.

The results reported in this paper reveal the critical importance of rapid mixing in the near field of the injectors. In the near field, the mixing rate is strongly dependent on the flowfield configuration. In the far field, however, the mixing of the injectant is governed by the rate of small-scale turbulent mixing. This suggests that the most effective means of increasing the overall rate of injectant mixing is to maximize the vortex generation and the jet-vortex interaction in the injector near field. Unfortunately, increasing the amount of vortex generation generally leads to increased total pressure losses. This presents a major tradeoff in many compressible mixing applications.

Acknowledgment

This work was supported by the NASA Langley Research Center under Grant NAG 1-795; G. Burton Northam was the technical monitor.

References

[1]McDaniel, J. C., "Quantitative Measurement of Density and Velocity in Compressible Flows Using Laser-Induced Iodine Fluorescence," AIAA Paper 83-0049, Jan. 1983.

[2]Hiller, B. H., and Hanson, R. K., "Simultaneous Planar Measurements of Velocity and Pressure Fields in Gas Flows Using Laser-Induced Fluorescence," *Applied Optics*, Vol. 27, No. 1, 1988, pp. 33–48.

[3]McDaniel, J. C., "Investigation of Laser-Induced Iodine Fluorescence for the Measurement of Density in Compressible Flows," Ph. D. Dissertation, Dept. of Aeronautics and Astronautics, Stanford Univ., Stanford, CA, Jan. 1982.

[4]Fletcher, D. G., and McDaniel, J. C., "Laser-Induced Iodine Fluorescence Technique for Quantitative Measurement in a Nonreacting Supersonic Combustor," *AIAA Journal*, Vol. 27, No. 5, 1989, pp. 575–580.

[5]Hartfield, R. J., Abbitt, J. D., and McDaniel, J. C., "Injectant Mole Fraction Imaging in Compressible Mixing Flows Using Laser-Induced Iodine Fluorescence," *Optics Letters*, Vol. 14, No. 16, 1989, pp. 850–852.

[6]Abbitt, J. D., Hartfield, R. J., and McDaniel, J. C., "Mole-Fraction Imaging of Transverse Injection in a Ducted Supersonic Flow," *AIAA Journal*, Vol. 29, No. 3, 1991, pp. 431–435.

[7]Hollo, S. D., Hartfield, R. J., and McDaniel, J. C., "Injectant Mole Fraction Measurements of Transverse Injection in Constant Area Supersonic Ducts," AIAA Paper 90-1632, June 1990.

[8]Fletcher, D. G., "Spatially-Resolved, Nonintrusive Measurements in a Nonreacting SCRAMJET Combustor Using Laser-Induced Iodine Fluorescence," Ph.D. Dissertation, Dept. of Mechanical and Aerospace Engineering, Univ. of Virginia, Charlottesville, VA, Jan. 1989.

[9]McDaniel, J. C., "Laser Methods for Nonintrusive Measurement of Supersonic Hydrogen-Air Combustion Flowfields," *Proceedings of the International Conference on the Applications of Lasers and Electro-Optics*, edited by R. J. Adrian, Vol. 67, Laser Inst. of America, Santa Barbara, CA, 1988, pp. 209–218.

[10]Hollo, S. D., Hartfield, R. J., and McDaniel, J. C., "Planar Velocity Measurements in Symmetric Flowfields Using Laser Induced-Iodine Fluorescence," *Optics Letters* (submitted for publication).

[11]Hollo, S. D., "Planar Mole Fraction and Velocity Imaging of Compressible Mixing in a Nonreacting Mach 2 Combustor," Master's Thesis, Dept. of Mechanical and Aerospace Engineering, Univ. of Virginia, Charlottesville, VA, May 1991.

[12]Dancey, C. L., and Wang, J. A. , "Laser Doppler Measurements in a Mach 2 Flow over a Rearward-Facing Step with Staged Injection," NASA CR NAS1-18471-Task 32, Feb. 1991.

[13]McDaniel, J. C., Fletcher, D. G., Hartfield, R. J., and Hollo, S. D., "Staged Transverse Injection Behind a Rearward-Facing Step: A 3-D Compressible Test Case for Hypersonic Combustor Code Validation," AIAA Paper 91-5071, Dec. 1991.

[14]Thomas, R. H., Schetz, J. A, and Billig, F. S., "Gaseous Injection in High Speed Flow," Ninth International Symposium on Air Breathing Engines, Athens, Greece, Sept. 1989.

[15]Rogers, R. C., "A Study of the Mixing of Hydrogen Injected Normal to a Supersonic Airstream," NASA TND-6114, March 1971.

[16]Rogers, R. C., "Mixing of Hydrogen Injected from Multiple Injectors Normal to a Supersonic Airstream," NASA TND-6476, Sept. 1971.

[17]Fujimori, T., Kawai, M., Ikeda, H., Ando, Y., Ohmori, Y., Aso, S., and Fukada, M., "Numerical Prediction of Two and Three Dimensional Sonic Gas Transverse Injections into Supersonic Flow," AIAA Paper 91-0415, Jan. 1991.